A Novel High Throughput Root Phenotyping Protocol and Structure Using Lemna Tec 3D

JAMEEL AHMAD KHAN AND H. E. SHASHIDHAR

Department of Plant Biotechnology, College of Agriculture, UAS, GKVK, Bangalore - 560 065

E-mail: jameelbiotec@gmail.com

ABSTRACT

This study was aimed at designing and demonstrating utility of a novel and low-cost tool as an accessory to image root growth of rice seedling in automated Lemna Tec 3D Scanalyzer. The tool enabled with RFID chip, designed to hold at least three test tubes carried root system of seedlings of five rice genotypes grown in test-tubes containing in transparent medium. A total of 30 (5 varieties x 6 replications) test-tubes were prepared among which uncontaminated 15 capped test-tubes carrying seedlings of rice in three replications were used to characterize the root growth. Variability of roots existed and Bala genotype outperformed in root growth rate and total root area. Additional seven parameters were also tested for possible surrogates for root growth rate and total root area. These studies demonstrate that the tool developed as an accessory to imaging system can facilitate rapid root phenotyping. Also, this method can be employed to assess the genetic variation in responses to abiotic stresses such as drought that cause osmotic stress during early growth of crop plants. When combined with genotyping, this can also support discovery of useful genes associated with root system responses to osmotic stress.

Keywords: Phenomics, lemna tec 3D, scanlyzer, roots, rice, root tool, abiotic stress

GENETIC improvement of tolerance to drought is important for staple food crops like rice, which face long dry spells during their growth under rain dependent agro-ecologies (Tardieu *et.al.,* 2018). Much of the genetic gain in grain yield of crops has resulted from genetic improvement of structural traits including yield and yield components, which are placed above the land surface in contrast to root. It is increasingly realized that the further genetic gain in crop productivity is likely to result from improved root traits and the root is the primary port of entry for water and mineral molecules, which are critical for plant growth. The traits specifically associated with root system architecture are gaining importance recently (Lynch, 2018). Benefit of improvement in root system architecture has been clearly demonstrated through novel phenotyping and molecular biology intervention for drought tolerance (Uga *et al.*, 2013). Such breakthrough in agricultural research are highly essential for ensuring enhanced food production for ever growing world population (Nelson *et al.*, 2012) and also to encounter climate change by increasing efficiency of roots (Anon., 2014). This situation demands the need for high throughput, robust and cheap hardware and software platforms as traditional methods of phenotyping roots, such as excavation or washed soil cores destroys the architecture of the root system. Recently several novel techniques have been used to investigate root systemsnon-destructively by employing imaging technologies. These technologies use imaging in visible range of electromagnetic spectrum and also X-ray computed tomography (Paya *et al.*, 2015). The images of root acquired from both minirhizotron (Fitters *et al.,* 2018); Rootfly [www.ces.clemson.edu/wstb/rootfly/], RootView [www.mv.helsinki.fi/aphalo/RootView.html], and Roo Tracker [www.biology.duke.edu/rootracker] and also in the controlled environments have been used to understand the genetic variation in root system architecture-responses of plants.

Lemna Tec 3D is a state-of-the art phenomics platform for phenotyping responses of plants grown in pots under controlled environment. It supports phenotyping large number of plants particularly with focus on shoots. Built in features of this platform include image acquisition systems, image analysis system and data mining for interpretation about the

genetic variation for several traits. (Hairmansis *et al.,* 2014 and Guo *et al.*, 2017).

The identification of genes for root related traits (or any other traits) depends on the precision of phenotyping. Some successful examples in capturing root phenes includes Root System Architecture (RSA) to land on *DRO1* (Uga *et al.,* 2013) in rice. Modification of RSA could contribute to improvements of desirable agronomic traits such as yield, drought tolerance and resistance to nutrient deficiencies (Paez-Garcia *et al.,* 2015).

A novel and low cost accessory customized for imaging root system of rice (*Oryza sativa*) at early stages of development under controlled environment. This highly versatile phenotyping tool was aimed at improvement inphenotyping throughput for characterization of root growth with or without osmotic stress in the growth media.

MATERIAL AND METHODS

Plant material and experiment conditions

Rice (*Oryza sativa*) seeds of five accessions were surface sterilized initially two times with double distilled water followed by Ethanol wash (70%) for 1 min and then with 40 per cent sodium hypochloride, 0.1 per cent tween-20. Seeds were rinsed with sterile water till froth is removed completely and placed in growth chamber (darkness at 25 ^{0}C for 42 hours) to synchronize germination.

Six germinated and uniformly sized seeds were placed on surface of gel inside test-tubes (20 x 2.5 cm) containing 40 ml of ½ strength MS media (without growth hormones) supplemented with 0.2 per cent Gelrite in control and 5 per cent PEG with gelrite for inducing osmotic stress. Hence, each genotype was replicated six times in control (1/2 MS + Gelrite) and stress (1/2 MS + Gelrite + PEG). Among the six replicates, only three healthy and uniformly germinated tubes were mounted on root structures placed in greenhouse for imaging, which was maintained at 25-30 ^{0}C during day and 20-25 ^{0}C during night.

Design of tool to acquire image of root system architecture

Since the focus was on root system at early stages of growth, it was felt that a suitable accessory is essential to acquire the images, when the seedlings are moved into the imaging chamber of phenotyping platform.The tool was designed to hold sufficient number of test-tubes at a desirable height for acquisition of root image. The emphasis was on low cost without compromising quality of image attributes. As Lemna Tec imaging chamber is equipped with side camera, the tool was designed to allow capture of root image of each sample at different angle.

As the outline of structure was ready, the only focus was to implement the idea in developing a cheap and an efficient tool as an accessory for acquisition of root images. The final design presented included

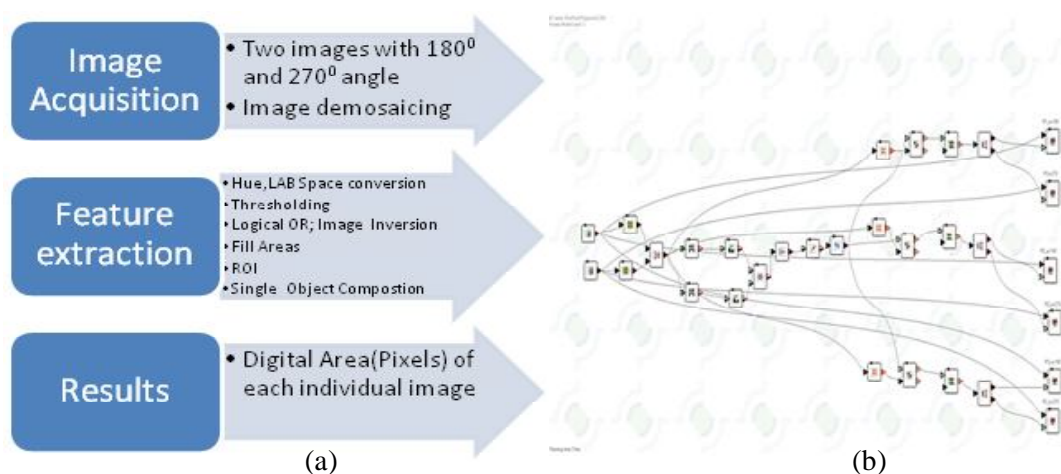(a)   (b)

Fig. 1: (a) Image processing steps; (b) Lemna Grid used to resolve image in present study

two EPVC pipes instead of mild steel tried at initial stage. The EPVC pipes were fixed on RFID tagged cars that were otherwise designed to carry pots. Nut and bolts were preferred to hold the structure upright and straight. The two EPVC pipes carried Medium-density fiberboard (MDF), which were drilled to accommodate three test tubes. This allowed diagonal placement of test tubes on the board for capturing images from four angles (0^0, 90^0, 270^0, 360^0).

Since the illumination inside the imaging chamber was not planned for root system architecture at seedling stage, the reflection added background noise while capturing the images. This could be avoided by using black cloth as background for each of the car. This substantially minimized the reflections and ensured clear differentiation of roots from background. Consequently, imaging was restricted to only two angles (90^0, 270^0) with three test-tubes for each of the cars for final imaging protocols (Fig. 2 i) details are given in Results and Discussion.

Imaging platform

LemnaTec Greenhouse Scanalyzer was used for root phenomics at ICAR-National Institute of Abiotic Stress Management (NIASM), Baramati, Pune which is otherwise used specifically for shoot phenomics.The conveyor system was employed to move the structure designed for facilitating the root imagesfrom growth rooms to imaging chamber without modifying the existing software. For non-invasive phenotyping, images of roots were captured through high resolution camera (piA2400-17gc CCD cameras by Basler, Ahrensburg, Germany) that senses the radiation in the visiblerange of the electromagneticspectrum. Prior to imaging, the inbuilt software was used to optimize image acquisition configuration for high resolution. While capturing the images the objects were illuminated by incandescent lights (FQ24W865HO or FH28W865HE, respectively, Osram GmbH, München Germany) placed on the top and at sides in the imaging chamber. The rotating platform in the chamber was used to capture the images from different angles (Fig. 2 II).

Feature extraction from images

Image processing is divided into three major parts: Image acquisition, Feature extraction and Results (Fig. 1a). Integrated Analysis Platform (IAP) of LemnaTec was followed for extracting features of root system. The analysis of image followed a particular flow from its capture to analysis as depicted in Fig. 1.

The image analysis grid had original image acquired from database with particular RFID tag for extraction of features of roots. The tools embedded in the image analysis grid have been described below (Fig. 2 III).

1. Two Raw images captured from different angles (180^0 and 270^0) were accessed using Database Reader (Fig. 2a).

2. Demonising of image was performed so as to convert Bayer pattern image into proper image color space.

3. Further batch mux was used for common image processing technique application.

4. Two image properties Hue from HSI Space and Blue Yellow Lab Space were fetched to apply threshold for both color image properties of an image (Fig. 2b-e).

Hue : 1 to 170 (Range from 0 to 255)
Saturation : 104 to 123 (Range from 0 to 255)

5. "Logical OR" of two threshold images was followed by image inversion (Fig. 2f).

6. In inverted image white represents objects of interest,whereas black indicates unwanted part of an image.

7. Small holes which were segmented as separate entity were filled by using Fill Area tool (Fig. 2g).

8. As original Image had three test-tubes three different Region of Interest (ROI) were defined (Fig. 2h).

9. Image ROI contains one or more image objects which were converted into single object using single object composition.

10. Lastly, each image object from each angle stored into database using DB Write tool (Fig. 2i).
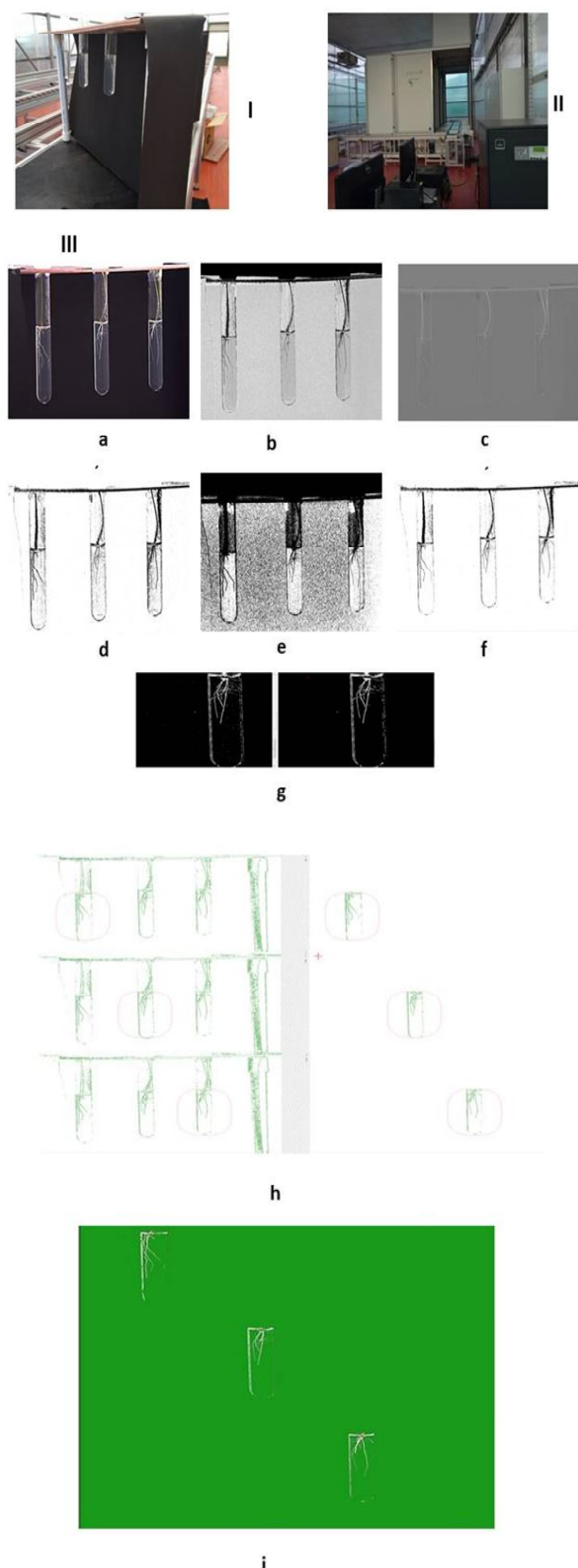
Fig 2: Overview of Imaging analysis. (I) A final structure with test-tube having 10 day old seedling.(II) Imaging chamber at LemnaTec facility ICAR-NIASM. (III) LemnaGrid analysis of raw image.
a)Original image captured; b)Hue property of image; c)Blue yellow LAB space of Image; d)Hue threshold; e) LAB threshold; f)Logical OR; g) Fill areas; h) Region of Interest (ROI); i) Final Skeleton of image

Quantification of root area

The final image mask is used to measure the size of the projected area of root by counting the number of image pixels. Pixels are surrogate measure of root area and consequently could be used for measuring root growth rate. Data obtained from the first day of imaging was subtracted from all days to obtain only root area (as pixels).

Data mining and analysis

A particular IAC number is assigned to each Lemna Grid (Fig. 1b) before using it for analysis of whole set of images acquired during the experiment. This helped in retrieving the data from database and export it to the Micro-Soft excel by using Lemna-Miner software. Descriptive statistics were used to differentiate the root system architecture of five genotypes.

Efficacy of tool developed for acquisition of seedling root system architecture

The major concerns to be addressed in comparing methods of root phenomics are the cost of structure and the quality of its output (Table 1). The tool

TABLE I

Approximate cost in time (person hours) for the three root screening methods for 38 genotypes.

Activity	Rhizotrons	Non-Woven Fabric	Hydroponics	EPVC Structure
Set Up	70	8	8	11 [d]
Sowing	4	4	8	12 [e]
Weekly maintenance	4	1	5	14 [f]
Harvesting	17 [a]	6	10	12
Post Harvesting	90 [b]	28 [c]	16	40 [g]
Cost	$60,000	-	-	$1-2 [*]
Total	185	47	47	89

a Includes 4 h to take photographs and 9 h weighing rhizotrons in the last 3 days.

b Includes 80 h root washing

c Includes 20 h root washing.

d Includes 5 hour test tube washing, 2 hour autoclaving, 2 hour media preparation and 2 hour pouring.

e Includes sowing in test tubes with six replications for each treatment (38x2x6)

f Includes everyday imaging for 2 hours

g Includes Image analysis using Lemna Grid

* This includes cost of materials for tool only

designed was cheaper than the most commonly used structure *i.e.,* rhizotrons or plexi-tubes suggested for root system investigations (Shrestha *et al.*, 2014). This could allow imaging of three samples from two angles at a time and helped in predicting root biomass after image analysis and data analysis. This also allows generation of time series data on root development by using LemnaTec conveyor and image acquisition chambers which is otherwise not possible with conventional tools particularly when number of genotypes to be phenotyped are large. In addition, the overall expenses of root phenotyping at seedling stage appear to be lower as compared to rhizotrons.

Quality of image acquired by the tool

Initially imaging protocol was done with six test-tubes at all four angles *i.e.,* 0^0, 90^0, 270^0, 360^0 (Fig. 3a-d) but the results seem in conclusive because of the image resolution. Image analysis platform could not properly separate foreground and background (Fig. 3e), which is the primary criteria for high-throughput analysis (Iyer-Pascuzzi *et al.,* 2010). The final image obtained (Fig. 3e) were not suitable for segmentation of the root system mainly because of background noise
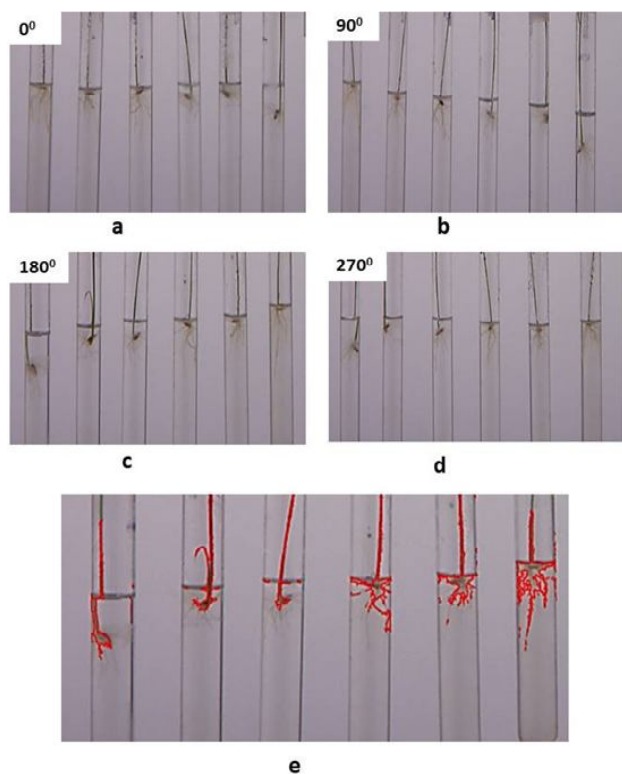

Fig 3: Image Analysis using all four angles at a) 0^0, b) 90^0, c) 180^0, d) 270^0 and e) Final image obtained after IAC

created by reflection from surface of the glass tubes and hence did not provide the appropriate pixels corresponding to root area. It was also observed that the area of root skeleton obtained with this method was less the real root area.

To improve image quality and obtain a proper foreground and background resolution, a black cloth was kept in the visible chamber exactly behind the capture area to diffuse reflectance (Fig. 4a-d). Images of roots in six test-tubes were captured from four angles. The quality of image improved substantially due to reduction in background noise except for reflections at the walls of test-tube. Hence, the skeleton area obtained by image analysis configuration was more than the real root area (Fig. 4e).
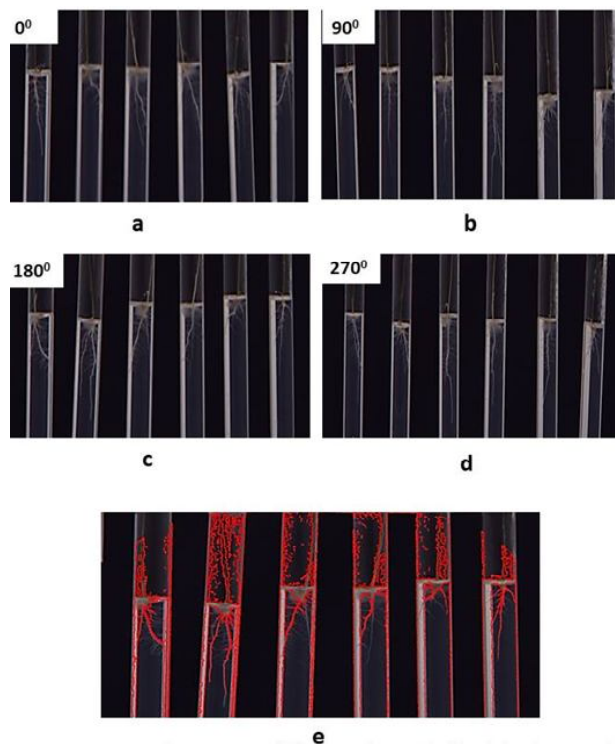
Fig 4: Image Analysis using all four angles with black background at a) 0^0, b) 90^0, c) 180^0, d) 270^0 and e) Final image obtained after IAC

To resolve this issue, technical errors in previous image analysis pipelines were corrected and a final structure was designed with permanent black background for each of the car carrying only three test-tubes instead of six tubes. However, this reduced the number of angles to only 90^0 and 180^0 only (Fig. 5a, b). This was the final trade-off which we could afford to obtain a quality image of roots of rice seedlings with minimum reflection (Fig. 5 c).
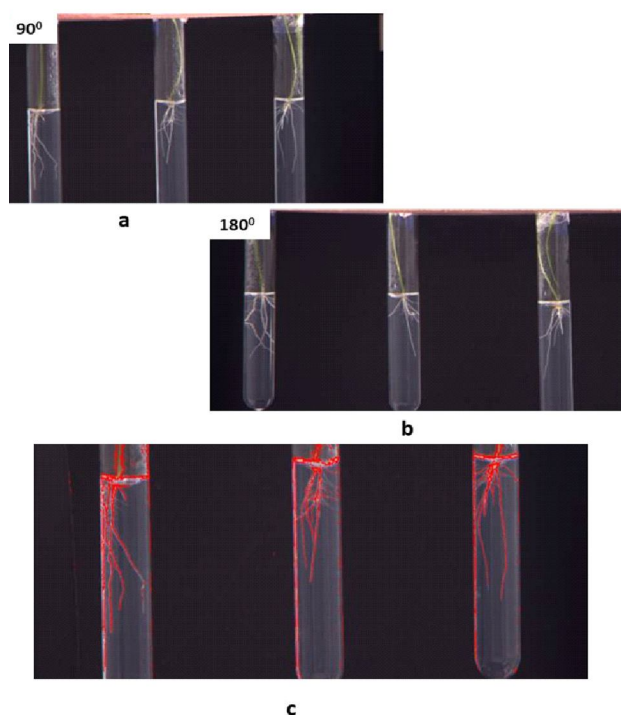
Fig 5: Image Analysis with only two angles with black background at b) 90⁰, c) 180⁰ and e) Final image obtained after IAC

In monocot plants, the rapid growth rate of plant and the lateral root development of the primary and embryonic crown roots are critical for early seedling vigor, especially during stress conditions (Hochholdinger and Tuberosa, 2009). The small amount of reflection persisted throughout the experiment for each of the test tubes could be eliminated in the image analysis by subtraction from images captured on subsequent days. Thus, the accessory designed for facilitating images of root system architecture of the plants were made fully functional for assessing the genetic variation among the rice cultivar chosen for the study.

RESULTS AND DISCUSSION

Candidate surrogates for understanding genetic variations

Among the various parameters obtained from Lemna Grid analysis only eight parameters were found to be possible candidates to understand the genetic variability and differential response of genotypes. Each parameter was checked to differentiate the response on root growth under control and osmotic stress conditions.

a. Sum of boundary point count

This is the most basic aggregations which will collect and summarize point features within a set of boundaries. The input parameters must include points to be aggregated and aggregation area. A clear distinction of pixel count as a function of root area in control and stress conditions was observed using this parameter (TableII). Also, it was observed that pixel count increased with each day of increased growth.

However, overall difference of control and stress treatments for Budha was not observed either because of misaligned pixel count at boundary or enhanced growth of roots in stress condition (Graph 1).
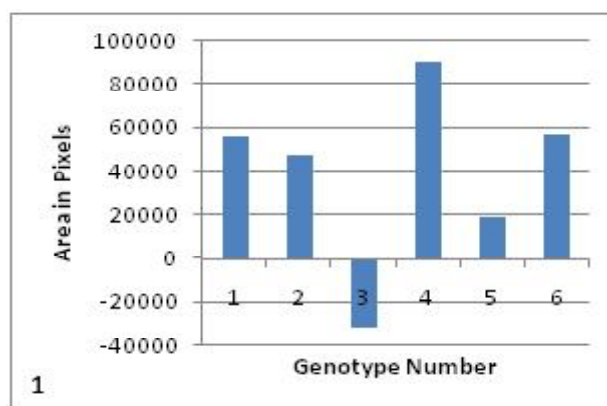
Graph 1: Overall difference of control and stress treatments for sum of boundary point count

b. Sum of boundary point roundness

This parameter more or less similar to previous one but focuses on effective way to compute the measure of circularity of a part of a digital boundary previously extracted from digital image. This parameter also gave a growth trend and distinction of control and growth conditions (Table II). Again, difference of control and stress from total pixel count for all the days showed Budha in negative count (Graph 2).

c. Sum of boundary points to area ratio

A derived parameter which gives a ratio of boundary points to the area layer to use for analysis. It can generate bins of a specific size and shape (hexagon or square) to aggregate into.

TABLE II

Sum of Boundary Point Count (BPC) and Sum of Boundary Point Roundness (BPR) for control and stress treatments among the selected genotypes

BPC	01		02		03		04		05		06	
	Control	Stress	Control	Stress	Control	Stress	Control	Stress	Control	Stress	Control	Stress
Day 0	18244	13648	18206	16221	13923	14590	18117	14157	15280	15112	16649	15826
Day 1	16368	12532	14248	16042	11870	14352	14599	13348	12150	14101	15284	15098
Day 2	18874	13866	19944	17669	15557	15825	21913	15441	17140	16266	20166	17077
Day 3	19500	14694	21916	19796	14356	18003	22836	15479	17670	17608	19389	16777
Day 4	21194	14154	27777	19341	17628	19442	27308	15816	22052	19872	23553	17636
Day 5	21458	16568	26132	20422	16450	21408	27168	16506	24306	21335	23373	16750
Day 6	22689	16267	28697	21979	18505	23081	29861	17485	27330	22672	25022	16832
Day 7	25132	19161	32368	24498	21222	24028	31677	18797	30622	25691	28503	18553
Day 8	22045	15845	28259	21005	18140	22988	28288	16882	26865	23382	25038	16014

BPR	01		02		03		04		05		06	
	Control	Stress	Control	Stress	Control	Stress	Control	Stress	Control	Stress	Control	Stress
Day 0	12116.557	10850.195	12508.371	12857.379	10091.415	11603.865	12656.481	11254.205	10925.106	11370.526	11904.191	12260.967
Day 1	10371.791	9847.3765	10885.915	12181.747	9068.679	10929.367	10606.021	10198.637	8893.0029	10260.192	10688.826	11162.21
Day 2	12041.54	11078.61	13033.109	13571.405	11117	12084.132	14042.946	12123.388	11945.284	11996.079	13689.163	12852.797
Day 3	12600.035	11481.37	16066.406	14980.526	10352.967	13618.412	16058.828	11997.332	12535.226	12860.22	13308.127	13218.648
Day 4	13329.447	10966.274	19786.851	14178.636	12515.393	14576.382	18504.424	11796.729	15187.399	14450.229	16671.842	13532.447
Day 5	13741.896	12622.78	19245.671	15152.115	11683.288	16209.091	19180.654	12685.8	18373.649	15800.432	16610.333	13127.049
Day 6	14351.744	12347.869	20899.456	16073.968	13126.223	17311.871	20793.886	13233.075	20544.932	16237.144	17757.941	12586.513
Day 7	15063.153	13418.37	21841.399	16917.767	13642.262	16614.326	19784.054	13316.309	21360.608	17245.115	19168.837	13310.54
Day 8	13761.539	11905.825	21009.149	15733.81	13026.904	16959.131	19628.145	12826.658	20176.639	16814.515	17843.359	11916.282
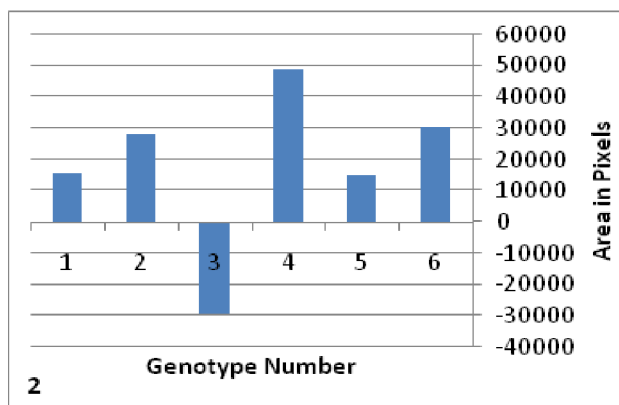
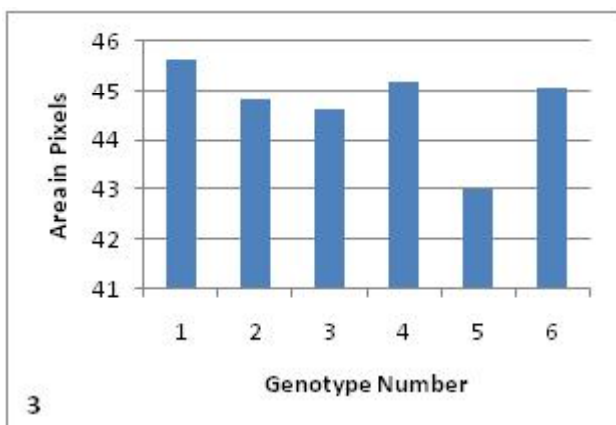Graph 2: Overall difference of control and stress treatments for sum of boundary point roundness

Growth rate difference between treatments (Table III), and clear distinction of differences showing Chenab and Budha to have more area under stress making this parameter most prominent candidate for selection purposes (Graph 3).
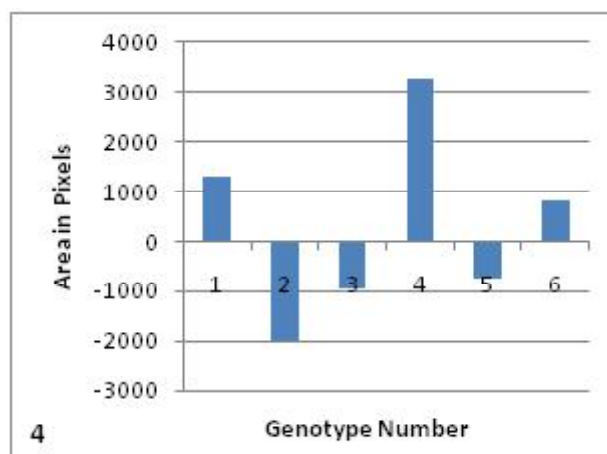

Graph 3: Overall difference of control and stress treatments for sum of boundary points to area ratio

d. Sum of caliper length

Caliper length gives the maximum length of skeleton obtained after processing the digital image. It can be used as a surrogate for root length.

Caliper length showed varied values in control and stress conditions amount the selected genotypes during the growth period of rice roots (Table III).

This surrogate could not capture the real root length probably because the reflection was taken as caliper length which exceeded the roots. However, improvements can lead to decreased noise and hence this parameter can be taken into picture. A negative value was obtained for few genotypes which included

Graph 4: Overall difference of control and stress treatments for sum of caliper length

the drought tolerant Bala, Budha (Graph 4). Either this could be missed pixel because of noise or could be deep rooting pattern of these genotypes as well.

e. Sum of circumference

The circle in the perimeter of the growing area gives an indirect indication of growth. This parameter is very effective in shoots where canopy is expected to widen with increased growth. Since there is no generalization for better parameter (widened root or narrow; deep or steep), therefore relying on this parameter is not effective.

Table IV, shows growth of roots for the growth period and its distinction for control and stress conditions. Also, Graph 5 predicts an overall growth difference with an exception of Chenab.
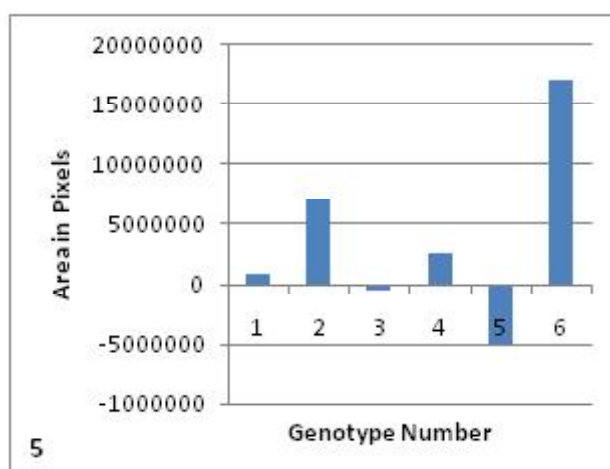
Graph 5: Overall difference of control and stress treatments for sum of circumference

TABLE III

Sum of Boundary Points (SBP) and Sum of Caliper Length (SCL) To Area Ratio for control and stress treatments among the selected genotypes

SBP	01		02		03		04		05		06	
	Control	Stress	Control	Stress	Control	Stress	Control	Stress	Control	Stress	Control	Stress
Day 0	3.9475064	4.7245332	4.0645285	4.7763155	4.4086961	4.7269255	4.1969116	4.7457517	4.3284835	4.4928901	4.229817	4.6304869
Day 1	3.7054557	4.603919	4.5533503	4.509112	4.6084273	4.539818	4.3801402	4.552219	4.3938866	4.2738558	4.1801033	4.3512933
Day 2	3.787015	4.7414	3.8993251	4.6469467	4.356267	4.4580541	3.8350264	4.6608107	4.2502179	4.4111979	4.0198318	4.515985
Day 3	3.8445589	4.6604231	4.371763	4.5603888	4.3906767	4.5178451	4.2089752	4.604394	4.3395077	4.3506479	4.0922368	4.73151
Day 4	3.7553698	4.6251661	4.2579395	4.4011495	4.3141165	4.4658556	4.0600516	4.4375738	4.188216	4.3285092	4.2275835	4.6108222
Day 5	3.8182511	4.5515367	4.4132949	4.4541501	4.3386225	4.5192526	4.2182094	4.5875895	4.5485201	4.4105269	4.2535067	4.7318362
Day 6	3.7733976	4.5651331	4.3601768	4.3813344	4.3119826	4.4892588	4.1640022	4.5214421	4.5105318	4.2772454	4.2561397	4.4887365
Day 7	3.5633088	4.2820483	4.0410925	4.1556451	3.8586581	4.1529783	3.7335797	4.2207926	4.1949314	4.0092731	3.9706113	4.2675685
Day 8	3.7152657	4.539956	4.4531648	4.4901824	4.3596823	4.4088411	4.1312115	4.5616237	4.479395	4.2688179	4.2872712	4.457703

SCL	01		02		03		04		05		06	
	Control	Stress	Control	Stress	Control	Stress	Control	Stress	Control	Stress	Control	Stress
Day 0	464238	426978	459279	438400	520477	485691	449148	414557	413969	455244	506239	503372
Day 1	449465	459311	430331	463643	494702	538068	485175	406324	376597	434093	455887	533237
Day 2	465627	484624	458384	446197	523153	500476	440216	447878	398397	467415	486468	465665
Day 3	467341	526695	438885	453401	512718	478214	478736	426940	397192	457572	510466	455980
Day 4	470165	468110	449947	474455	531677	493448	531972	408337	398249	487663	554174	447135
Day 5	455701	466012	425810	443258	481607	519853	489615	415013	397175	433739	459170	462733
Day 6	464983	506584	441149	455427	486097	479816	551744	460757	429215	471073	470538	444999
Day 7	491443	507146	471010	478930	460977	448031	521520	448690	428912	449617	453712	474717
Day 8	482562	411754	452335	442448	510655	541102	551003	421290	392603	408500	492388	450569

f. Sum of convex hull area

Convex hull is the closure of set of *X* points in an Euclidean plane with the smallest convex set that contain *X*.

All the selected genotypes were captured using this surrogate. Table IV shows the differential growth pattern in treatments along the growth period.

Graphical representation of subtractive interpretation was found to be effective in Chau, as it might not have performed well under osmotic stress (Graph 6).
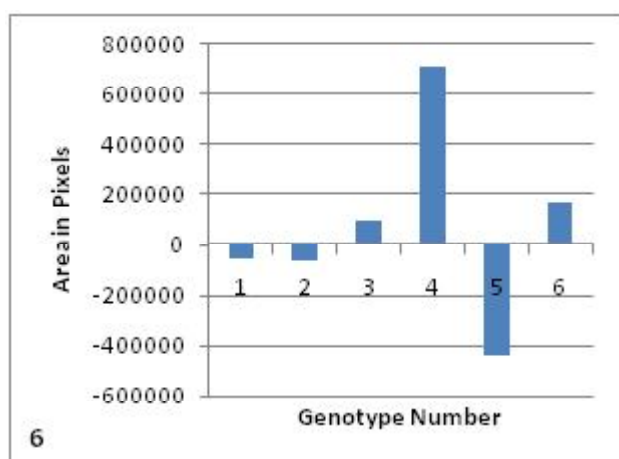
Graph 6 : Overall difference of control and stress treatments for sum of convex hull area
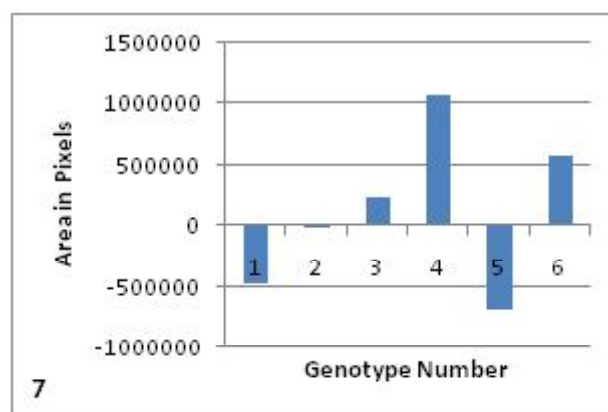
g. Sum of min area rectangle area

After the circular enclosure with different parameters around the region of interest, a rectangular area can also help in calculating the growth of roots.

Root growth and its consequent difference under stress was captured and translated to data which is presented in Table V.

Chau again seemed to perform well in control condition whereas; Chenab genotype was maximum rectangular area under osmotic stress.

An efficient correspondence between real and reel shoot area has been reported previously with the main interest to capture exponential growth phase (Fiorani and Schurr, 2013). Many of the surrogate parameters failed to deliver for root parameters. However, detailed investigation need to be followed for the noise reduction and post-processing to yield

more parameters for study. Phenotyping platforms and its analysis that can identify small differences can help in selection of desired traits in a given population. To access variable growth rates and differences under control and stress conditions, area through the pixel count was considered as most promising surrogate.

Graph 7: Overall difference of control and stress treatments for sum of min area rectangle area

Genetic variations observed in rice genotypes *vis-a-vis* root area

To prove the efficacy of our imaging tool, Lemna Tec 3D conveyer system helped in capturing the images of five genotypes with three replications grown on gelrite and MS media. It was found that Arnoliswee and Pokali had more area at the end of experiment. This was expected as Arnoliswee is drought tolerant and Pokali is salt tolerant genotype, hence much of the biomass during in these two varieties of rice was devoted towards root growth. The highest growth rate was observed in Bala, Chenab and Chau (Fig. 6a). This depicts a genetic variation in total root mass acquired by plant as well as growth rate among the rice genotypes.

We also compared the growth of Arnoliswee in Poly ethylene glycol (PEG) and found the significant reduction in growth rate and the final area relative to untreated plants (Fig. 6b). PEG is often used to create osmotic stress in experiments aiming at drought tolerance or salt tolerance in crop plants (Hasanuzzaman *et. al.,* 2017). Thus our study indicates that the tool developed for acquisition of root image and the protocol developed for acquisition and analysis of image can be used for screening responses of rice seedlings for drought tolerance.

TABLE IV

Sum of Caliper Length (SCL) and Sum of Circumference (SoC) for control and stress treatments among the selected genotypes

SCL	01		02		03		04		05		06	
	Control	Stress	Control	Stress	Control	Stress	Control	Stress	Control	Stress	Control	Stress
Day 0	75905.7926	40873.9928	188764.591	29756.2779	141113.626	90039.168	164645.361	19512.9191	212478.4391	27344.7428	70051.9014	12079.5982
Day 1	140489.6712	20251.0113	116707.497	115427.4398	12947.8535	64382.6558	72038.726	95227.3789	24150.8234	175456.5684	12115.6513	30563.69295
Day 2	18681.16	75753.0827	557710.418	224596.1619	81450.2241	79538.5512	385069.3421	9336.2875	144109.773	112471.9933	46186.419	155675.346
Day 3	3283.1549	115186.4972	460147.0048	193525.8055	60302.3601	44814.5754	177985.98	54294.9885	164166.6481	69403.2716	114981.646	95516.2975
Day 4	269203.182	451163.1027	6401966.242	56841.3053	116966.512	283979.698	402471.2612	1392.6977	607081.139	141442.9412	202486.715	17274.6749
Day 5	253369.7134	151676.293	342967.281	279199.5737	99573.6274	77921.2228	430363.5318	8756.8411	91132.2533	6038340.428	167450.168	218806.361
Day 6	261322.1109	161740.99	888822.824	441703.32	142198.0491	185083.7601	389206.55	252739.865	379243.7072	05217.4162	152091.2892	65203.4069
Day 7	215964.6388	324273.5829	350405.7929	294172.7285	230657.8428	1072.3055	563927.5746	49975.3866	04907.3364	34274.6081	7072062.1	166652.239
Day 8	75905.7926	40873.9928	188764.591	29756.2779	141113.626	90039.168	164645.361	19512.9191	212478.4391	27344.7428	70051.9014	12079.5982

SoC	01		02		03		04		05		06	
	Control	Stress	Control	Stress	Control	Stress	Control	Stress	Control	Stress	Control	Stress
Day 0	464238	426978	459279	438400	520477	485691	449148	414557	413969	455244	506239	503372
Day 1	449465	459311	430331	463643	494702	538068	485175	406324	376597	434093	455887	533237
Day 2	465627	484624	458384	446197	523153	500476	440216	447878	398397	467415	486468	465665
Day 3	467341	526695	438885	453401	512718	478214	478736	426940	397192	457572	510466	455980
Day 4	470165	468110	449947	474455	531677	493448	531972	408337	398249	487663	554174	447135
Day 5	455701	466012	425810	443258	481607	519853	489615	415013	397175	433739	459170	462733
Day 6	464983	506584	441149	455427	486097	479816	551744	460757	429215	471073	470538	444999
Day 7	491443	507146	471010	478930	460977	448031	521520	448690	428912	449617	453712	474717
Day 8	482562	411754	452335	442448	510655	541102	551003	421290	392603	408500	492388	450569

TABLE V

Sum of Min Area Rectangle Area (MAR) for control and stress treatments among the selected

SCL	01		02		03		04		05		06	
	Control	Stress	Control	Stress	Control	Stress	Control	Stress	Control	Stress	Control	Stress
Day 0	512723	508622.29	507457.5	486009.21	652780.34	589603.53	519591.37	451232.98	447383.53	495037.96	645300.85	610094.44
Day 1	497071.99	549651.7	515715.97	529035.1	575893.25	663866.98	580432.52	455120.53	393279.24	477189.59	556550.49	638583.75
Day 2	515792.3	562231	534911.94	493523.82	649672.72	597595.42	480399.47	524589.05	413611.52	533871.43	601755.75	527533.76
Day 3	517566.31	650296.28	502683.1	500973.2	647586.53	555598.04	545574.85	474698.46	414316.39	493136.22	654284.28	505102.56
Day 4	518827.06	553995.75	501373.9	549132.56	652125.64	592832.46	637779.17	455183.78	413711.68	558788.15	741714.77	500708.8
Day 5	501959.56	545362.59	476018.23	493444.56	584122.5	649887.71	584546.46	446808.32	415610.81	486188.27	543328.52	521343.85
Day 6	514035.53	630462.58	499512.92	509653.94	587523.14	560062.96	680642.36	547979.11	472721.52	522315.91	555814.43	500288.57
Day 7	539142.73	586925.51	534573.58	536048.7	516348.48	477265.14	588615.51	497932.55	445400.54	484855.52	514576.8	523682.44
Day 8	566217.45	512511.89	505109.38	498806.89	632126.07	705898.51	693406.38	479874.18	413235.56	451679.64	567062.73	522427.36

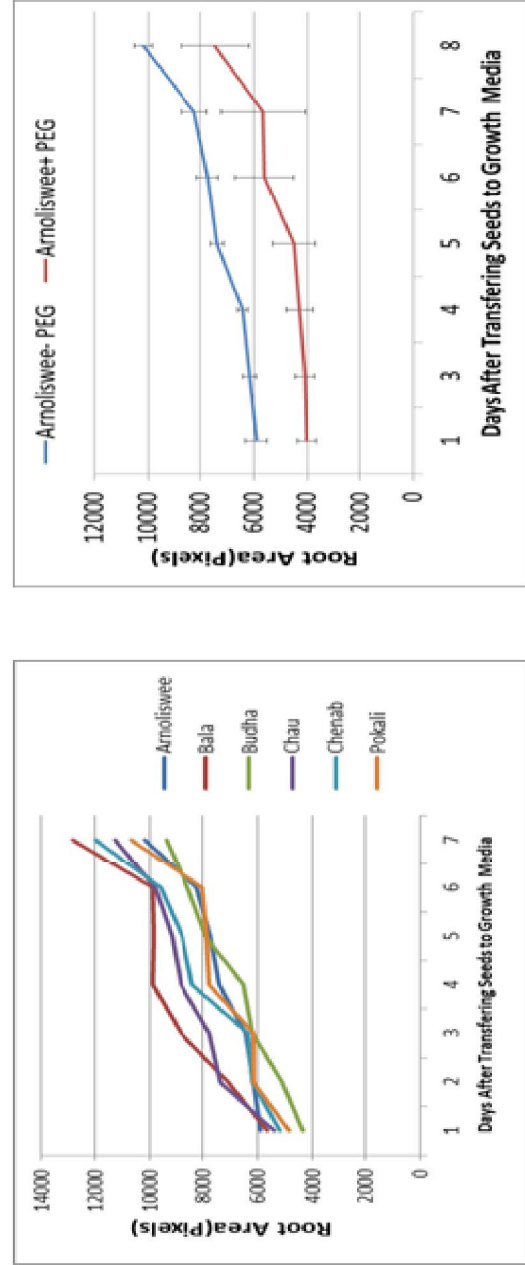1. ARNOLISWEE.
2. BALA
3. BUDHA
4. CHAU
5. CHENAB
6. POKALI

Fig. 6: (a) Relative growth rate of the genotypes used in study; (b) Difference in growth pattern in control(green) and stress(red) conditions

It has been found in analysis that root types are controlled by distinctly different genetic and developmental networks (Rebouillat *et al.*, 2009). The ability of this root imaging structure with LemnaTec platform can capture and track the differences among the genotypes with respect to spatial and temporal features of root system architecture. This can facilitate studies aiming at insight into the genetics of developmental changes that occur in the root system in response to different stresses. The main features of the tool designed and demonstrated for acquisition of imagein this study are (i) availability of transparent system to visualize roots; (ii) diagonally placed test-tubes to acquire images from more than one angle; and (iv) The low costmaterial for repeated use.

We have presented a novel tool and protocol for facilitating root phenotyping for crops like rice in high through-put Lemna Tec facility. This protocol in combination with in-built Lemna Grid software can enable acquisition and analysis of high quality images of roots. This can help in differentiating root responses of germplasm when subjected to stress.

Currently available phenomics tools for roots share many things especially for gel based medium and image resolution pattern to obtain a 3D skeleton model of roots. We used artificial growth media (gelrite with MS media) with and without PEG to give a vivid observation of drought strategies of genotypes. The materials used in developing structure and the constituents of media are readily available at cheap rate. Our protocol meets the end of medium- to high throughput handling of root images with the restriction of obtaining complexity in root structure.

References

Anonymous, 2014, Intergovernmental panel on climate change. Contribution of working group I to the Fifth Assessment Report of the Intergovernmental Panel on Climate Change. *The Physical Science Basis.* Cambridge University Press, New York, pp. 1535.

Fiorani, F. and Schurr, U. 2013, Future scenarios for plant phenotyping. *Annu. Rev. Plant Biol.,* **64** : 267 - 291.

Fitters, T. F., Mooney, S. J., and Sparkes, D. L. 2018, Sugar beet root growth under different watering regimes: a minirhizotron study. *Environ. Exper. Bot.,* **4** (2) : 322.

Guo, D., Juan, J., Chang, L., Zhang, J. and Huang, D., 2017, Discrimination of plant root zone water status in greenhouse production based on phenotyping and machine learning techniques. *Scientific Reports,* **7** (1) : 8303.

Hairmansis, A., Berger, B., Tester, M. and Roy, S. J., 2014, Image-based phenotyping for non-destructive screening of different salinity tolerance traits in rice. *Rice,* **7** (1) : 16.

Hasanuzzaman, M., Shabala, L., Brodribb, T. J., Zhou, M. and Shabala, S., 2017, Assessing the suitability of various screening methods as a proxy for drought tolerance in barley. *Functional plant biology,* **44** (2) : 253 - 266.

Hochholdinger, F. and Tuberosa, R., 2009, Genetic and genomic dissection of maize root development and architecture. *Current opinion in plant biology,* **12** (2) : 172 - 177.

Iyer-Pascuzzi, A. S., Symonova, O., Mileyko, Y., Hao, Y., Belcher, H., Harer, J., Weitz, J. S. and Benfey, P. N., 2010, Imaging and analysis platform for automatic phenotyping and trait ranking of plant root systems. *Plant physiology,* **152** (3) : 1148 - 1157.

Lynch, J. P., 2018, Rightsizing root phenotypes for drought resistance. *J. experimental botany,* ery 048.

Nelson, W. J., Lee, B. C., Gasperini, F. A. and Hair, D. M., 2012, Meeting the challenge of feeding 9 billion people safely and securely. *J. Agromed.,* **17** : 347- 350.

Paez-Garcia, A., Christy, M. M., Wolf-Rudiger, S., Rujin, C., Elison, B. B. and Maria, M. J., 2015, Root traits and phenolyping strategies for plant improvement. *Plants,* **4** (2) : 334-355.

Paya, A. M., Silverberg, J. L., Padgett, J., and Bauerle, T. L., 2015, X-ray computed tomography uncovers root–root interactions: quantifying spatial relationships between interacting root systems in three dimensions. *Front Plant Sci.,* **6** : 274.

Rebouillat, J., Dievart, A., Verdeil, J. L., Escoute, J., Giese, G., Breitler, J. C., Gantet, P., Espeout, S., Guiderdoni, E. and Périn, C., 2009, Molecular genetics of rice root development. *Rice,* **2** (1) : 15.

Shrestha, R., Al Shugeairy, Z., Al Ogaidi, F., Munasinghe, M., Radermacher, M., Vandenhirtz, J. and Price, A. H., 2014, Comparing simple root phenotyping methods on a core set of rice genotypes. *Plant Biology,* **16** (3) : 632 - 642.

Tardieu, F., Simonneau, T. and Muller, B., 2018, The physiological basis of drought tolerance in crop plants: A scenario-dependent probabilistic Approach. *Annual review of plant biology,* (0).

Uga, Y., Sugimoto, K., Ogawa, S., Rane, J., Ishitani, M., Hara, N. and Inoue, H., 2013, Control of root system architecture by *DEEPER ROOTING 1* increases rice yield under drought conditions. *Nature genetics,* **45** (9) : 1097.